describing the change in the population of this level corresponds to the relaxation channel (2.1). If the initial system of constants [4] is taken, then the subsequent evolution of the population of the level $(10°0, 02°0)^{I}$ will depend simultaneously on both the relaxation over the channel (2.1) and relaxation over the channels (2.2), (2.3). If leakage of vibrational quanta occurs over channel (2.1), then filling the level $(10°0, 02°0)^{I}$ will occur over channels (2.2) and (2.3), which results in the long run in equilibrium of these oppositely directed processes and the achievement of the minimum on the curve $n_2(t)$.

The model used in this paper for vibrational relaxation certainly needs correction in order to take more complete account of the processes in the initial stage. The process of emptying the level $(10°0, 02°0)^{II}$ because of radiation, the process of rotational relaxation if it is also prolonged in nature, requires simultaneous examination in studying the vibrational relaxation between the levels $(10°0, 02°0)^{I}$ and $(10°0, 02°0)^{II}$.

LITERATURE CITED

1. E. R. Murray, C. H. Kruger, and M. Mitchner, "Vibrational nonequilibrium in carbon dioxide electric discharge lasers," J. Chem. Phys., 62, No. 2 (1975).
2. K. Herzfeld, "Deactivation of vibrations by collision in the presence of Fermi resonance," J. Chem. Phys., 47, No. 2 (1967).
3. K. N. Seeber, "Radiative and collisional transition between coupled vibrational modes of CO_2," J. Chem. Phys., 55, No. 10 (1971).
4. R. D. Sharma and C. A. Brau, "Energy transfer in near-resonant molecular collisions due to the long-range forces with application to transfer of vibrational energy from the ν_3 mode of CO_2 to N_2*," J. Chem. Phys., 50, No. 2 (1969).
5. N. V. Karlov, Yu. B. Konev, I. V. Kochetov, and V. G. Pevchov, "Kinetic processes in a system of low CO_2 molecule levels," Preprint No. 183 [in Russian], FIAN SSSR, Moscow (1976).
6. R. R. Jacobs, K. J. Pettipiece, and S. J. Thomas, "Rate constants for the CO_2 02°0-10°0 relaxation," Phys. Rev., 11A, No. 1 (1975).
7. B. V. Egorov and V. N. Komarov, "Features of vibrational relaxation of a CO_2–N_2 mixture, described by a four-temperature kinetic model," Tr. TsAGI, No. 2177 (1982).
8. T. A. De Temple, D. R. Suhre, and P. D. Coleman, "Relaxation rates of lower laser levels in CO_2," Appl. Phys. Lett., 22, No. 8 (1973).

ENERGY ACCOMMODATION FOR GAS IONS ON A POLYCRYSTALLINE MATERIAL

V. A. Shuvalov

UDC 533.932.533.601.18

The interaction between a body and a low-density gas flow is largely characterized by the coefficients for the exchange of momentum and energy or the equivalent accommodation coefficients, the latter being used in determining convective heat fluxes and aerodynamic characteristics under free-molecular flow conditions, and they are important elements in the working relations no matter what the scheme used for the reflection of the gas atoms by the surface (specular-diffuse scattering, isolated reflection, Shamberg's model, Nochill's model, etc.).

The most detailed theoretical studies have been made of the interaction between gas atoms with clean crystalline structures. There are many papers on the simulation of collisions between atomic particles and surfaces, which give approximate analytic solutions characterizing the mechanisms for momentum and energy transfer from the gas atoms to ideal crystalline surfaces [1, 2].

Dnepropetrovsk. Translated from Zhurnal Prikladnoi Mekhaniki i Tekhnicheskoi Fiziki, No. 6, pp. 17-25, November-December, 1983. Original article submitted September 6, 1982.

0021-8944/83/2406-0778$07.50

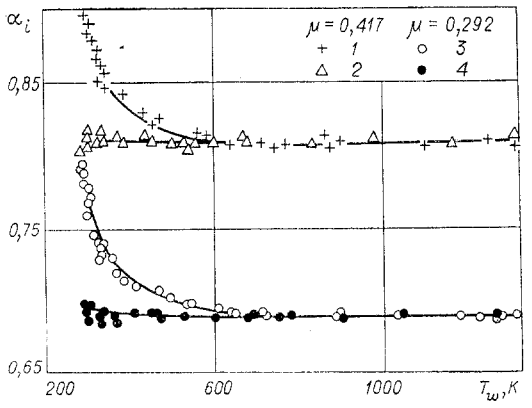

Fig. 1

In practice, a target with an ideal single-crystal structure is very rare. In most cases, the target has a polycrystalline structure [3]. The literature also lacks the necessary volume of information on the accommodation coefficients for gas molecules on the polycrystalline materials for the energy range of 1-100 eV, which is of importance from the viewpoint of aerodynamics. It is therefore important to study the transfer of energy and momentum by various gas-polycrystalline systems in this energy range.

Here we present results from an experimental study of various factors characterizing the interaction between a gas and a surface on the energy accommodation coefficients for gas ions of atomic mass from 4 to 131 on polycrystalline surfaces.

The energy accommodation coefficient α_i, the work function $\varkappa$, and the secondary ion-electron emission coefficient γ_i largely characterize the heat fluxes transported by gas ions to a conducting surface in a low-density medium:

$$Q_i = \frac{I_i}{e}\{h_i - \varkappa(1+\gamma_i) + \alpha_i[W_i + (e|V| + \chi)]\}.$$

In [4], the following equations were derived from the energy-balance equation for points on the temperature characteristic $T_w = T_w(V)$ with equal temperatures at different potentials $T_w^A(V^A < 0) = T_w^B(V^B > 0)$ for the thermoanemometric probe:

$$\alpha_i = \frac{h_i + (1+\gamma_i)(W_e + e|V^B|)}{W_i\{I_{0i}/I_i^A - [1 + (e|V^A| + \chi)/W_i] + (1+\gamma_i) I_{0i}/I_e^B\}}; \quad (1)$$

$$\varkappa = \frac{h_i - (W_e + e|V^B|)\{1 - [1 + (e|V^A| + \chi)/W_i] I_i^A/I_{0i}\} I_e^B/I_i^A}{1 + \gamma_i + \{1 - [1 + (e|V^A| + \chi)/W_i] I_i^A/I_{0i}\} I_e^B/I_i^A}, \quad (2)$$

which relate the parameters α_i, $\varkappa$, and γ_i; here h_i is ionization potential, W_α is the energy transported by particles of type α to the plasma-layer surface, I_α is the probe current, V is the potential difference passed by a particle in the layer near the electrode, I_{oi} is the saturation ion current to the probe oriented along the normal to the velocity vector of the flow ($\theta = 0$), $\chi = 3.6/d$ is the polarization energy, and d is the distance from the surface of the target at which the positive ions are neutralized. For most surfaces and ions in the above energy range, $d \approx (2-4)\cdot 10^{-7}$ mm [5]. With an error of not more than ~±10%, d can be found as half the sum of the diameter of a gas molecule as calculated from the viscosity and the distance between target lattice atoms.

As $\varkappa$ is independent of the type of particle, and $\gamma_i \ll 0.1$ for the xenon–metal systems [5, 6], it is convenient to use (2) to determine $\varkappa$ on bombardment by Xe^+. This enables one to use identical conditions at the surface and employ (2) to determine the secondary-emission coefficient γ_i on bombardment of the target by other gases with $\gamma_i \gtrsim 0.1$.

These values of γ_i can be used to monitor surface cleanness [6, 7] and to determine energy accommodation coefficients by means of (1).

The experiments were performed with a plasma gasdynamic system in a flow of partially ionized gas generated by a gas-discharge accelerator with electron-impact ionization. The working gases were helium, neon, nitrogen, argon, krypton, and xenon of the highest purity. The accelerated ion beam of intensity $j_\infty \approx 10^{17}$ ion/cm^2·sec enters the working chamber, in

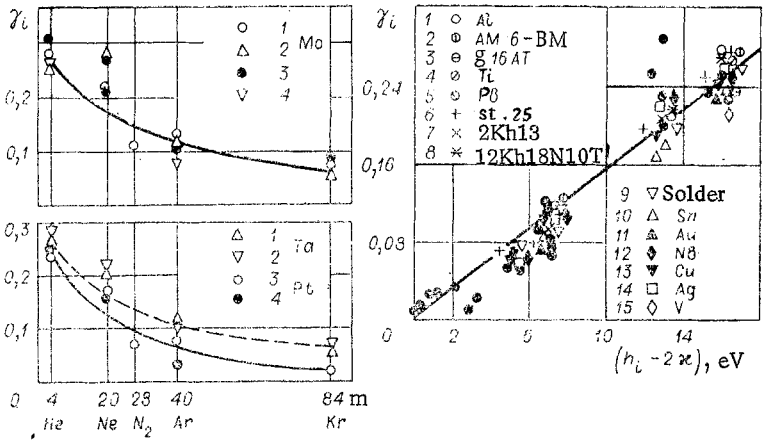

Fig. 2

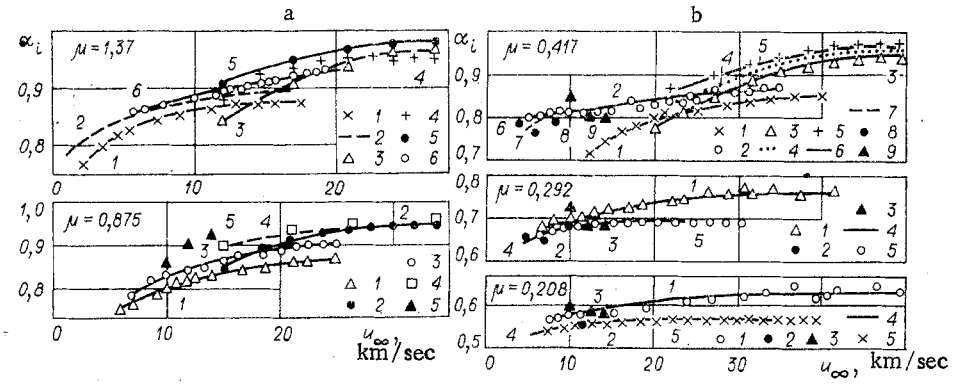

Fig. 3

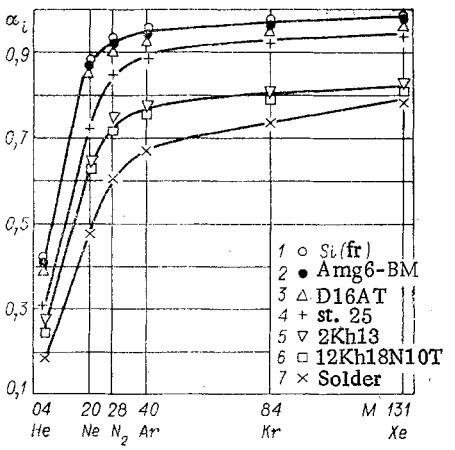

Fig. 4

which the residual-gas pressure was $\sim(0.9 - 1.3)\cdot10^{-4}$ Pa. The measurements were made at a pressure of $\sim(1.16 - 2.1)\cdot10^{-3}$ Pa. We used a planar thermoanemometer probe in the form of a disk $\delta \approx 0.12$ mm having a working surface of diameter about 3.5 mm with a thermocouple and the current lead connected to the rear surface. The side surfaces of the transducer, thermocouple, and current lead were insulated from contact with the plasma by a ceramic tube. The transducer was calibrated in the thermostate before use to determine $T_w = T_w(E)$, where E is the thermocouple emf.

The probes were made of pure metals with atomic masses from 27 to 207 and had polished working surfaces, as well as from engineering materials such as AMg6-BM and D16AT aluminum alloys (rolling), stainless steels 12Kh18N10T and 2Kh13, steel 25, and an element from a

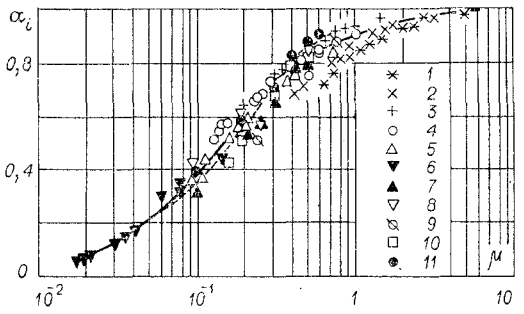

Fig. 5

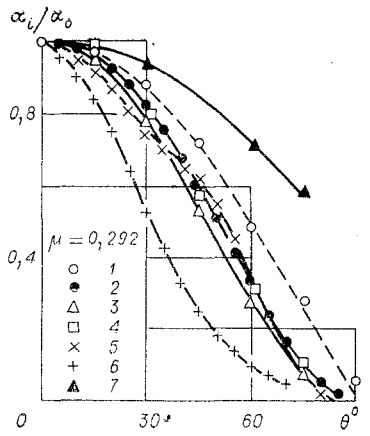

Fig. 6

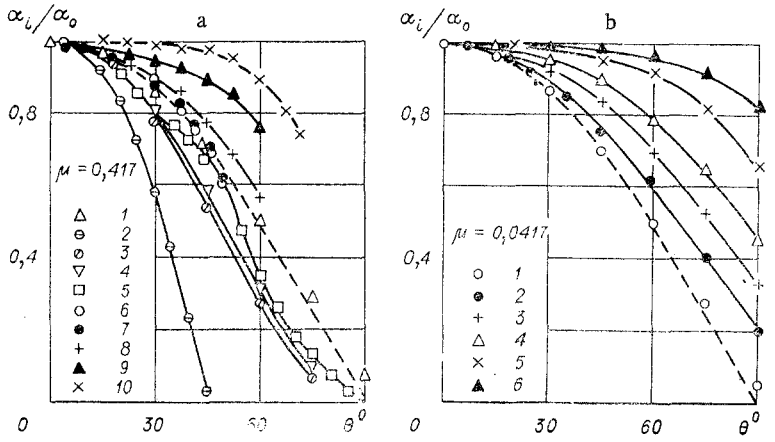

Fig. 7

solar-battery panel. The last was used in making two transducers: a silicon element (a polished piece of polycrystalline silicon doped with arsenic or phosphorus from the front surface of the panel) and a solder one (lead–tin alloy, shadow side of panel). The surfaces of the engineering-material transducers corresponded to the working states of these materials [8].

The row of transducers was placed in a high-speed flow of low-density plasma. The voltage–current characteristics were processed in the usual way [9]. The energy of the ions was determined with a multielectrode analyzer probe and also from the potential difference between the two peaks on the electron part of the voltage–current characteristic for a planar probe [10]. The plasma potential was determined by the second-derivative method and also from the electron part of the probe characteristic plotted on a semilogarithmic scale. This gave high accuracy in measuring the energy of the ions W_i. The values of W_i were calculated on the assumption that the accelerating potential was equal to the difference between the potential of the anode in the source and the local plasma potential, and they agreed satisfactorily with data obtained with the multielectrode analyzer probe as well as with the W_i found from the potential difference between the two peaks on the electron branch of the probe characteristic. The spread in the values of W_i was not more than ±4.5%. The local values of the working parameters were checked along with the orientation of the transducers with respect to the flow-velocity vector by means of a thin cylindrical probe made of molybdenum wire of diameter 0.04 mm and length 2.3 mm. The peak in the ion current measured by this probe on rotation around vertical and horizontal axes corresponds to orientation of the probe along the flow [11].

Particular attention was given to cleanness in the working surfaces of the probes. Directly before the measurements, the working surfaces were run in by bombardment with the plasma flow.

Figure 1 illustrates the effects of probe surface temperature and plasma flow intensity on α_i for argon and nitrogen at $u_\infty \approx 10$ km/sec on Mo. The points on the $T_W = T_W(V)$ curve were taken in such a way that $(e|V^A| + \chi) \ll W_i$. The probe was heated to high temperatures by Joule heating. The points on curves 1 and 3 show the results for α_i in a plasma flow of intensity $j_\infty \approx 10^{13}$ ion/cm^2•sec (charged-particle concentration $n_0 \approx 10^7$ cm^{-3}). The points on curves 2 and 4 correspond to a flow of intensity $j_\infty \approx 10^{17}$ ion/cm^2•sec ($n_0 \approx 10^{11}$ cm^{-3}).

For a probe surface temperature $T_W \approx 300°K$, the data of Fig. 1 illustrate the effects of flow intensity and adsorbed layer on α_i for argon and nitrogen ions striking polycrystalline molybdenum.

The sources of the adsorbed layer may be the gas (Ar or N_2) and the residual gas in the working chamber. Mass spectroscopy showed that two components predominated in the residual gas: water vapor (H_2O) and CO + N_2. There were also small amounts of H_2 and CO_2. A residual gas similar in composition was observed in the vacuum chamber of [12]. The working chamber in this plasma system had additional trapping surfaces cooled by liquid nitrogen although the pumping parameters were similar in other ways to those of [12].

Not much is known about the desorption of CO from Mo. The adsorption of CO on W has been examined in more detail. The published data on the adsorption of CO, N_2, H_2, and other components on W and Mo show appreciable similarities, which is to be expected because W and Mo belong to the same group of transition metals and the lattice constants are identical. In the CO—W(100) system, the desorption spectrum for the initial layer is qualitatively similar to that for polycrystalline tungsten in that in both cases there are pronounced peaks corresponding to the α component at $T_W \approx 200$-$450°K$ and the β state at $T_W \approx 850$-$1226°K$. In the desorption of CO from molybdenum, there are analogous adsorbed states, but with lower desorption energies. Similarity is observed also in the desorption of N_2 and H_2 from W and Mo [3]. The desorption of water vapor H_2O occurs at 450-670°K [12, 13].

The inert gases are either not adsorbed at all on W and Mo or are only very slightly [14].

In [15], measurements were made of the energy accommodation coefficients for Ar, Ne, and He from room temperature upwards, and almost complete desorption of films of N_2 and H_2 from polycrystalline tungsten was found at surface temperatures of about 600-650°K.

The data indicate that the values of α_i for Ar^+ and N_2^+ as measured on polycrystalline molybdenum (Fig. 1) at $T_W \geq 600°K$ (Ar^+), $T_W \geq 700°K$ (N_2^+), and $u_\infty \approx 10$ km/sec correspond to clean targets. When the target is bombarded at $j_\infty \approx 10^{17}$ ion/cm^2•sec, similar values were obtained at $T_W \approx 300°K$. The ion branch of the probe characteristic was recorded beginning with negative potentials of about —50 V, which slightly exceeds the threshold values for the sputtering energy of polycrystalline molybdenum [6]. As the negative potential was increased to —250 V, bombardment at $j_\infty \approx 10^{17}$ ion/cm^2•sec did not produce any changes in $\alpha_i^{Ar^+}$ and $\alpha_i^{N_2^+}$ at $T_W \approx 300°K$. Moreover, the same values of α_i at $T_W \approx 300°K$ were obtained also on bombarding the surface of the probe with a plasma flow of intensity $j_\infty \approx 10^{15}$-10^{16} ion/cm^2•sec, when the ion branch of the voltage—current characteristic was recorded starting at —200 to —250 V.

Figure 1 for $T_W \approx 300°K$ illustrates the effects of the adsorbed layer on the transfer of energy from Ar^+ and N_2^+ to polished polycrystalline molybdenum in normal incidence with $u_\infty \approx 10$ km/sec for the case $\mu \geq \mu_1$, where μ is the ratio of the masses of the gas and target atoms and μ_1 is the ratio of the masses of the adsorbed atoms and the target. The tendency for α_i to increase in the presence of the adsorbed layer at $\theta \approx 0$ agrees qualitatively with the estimates of [16] made with $\mu = 0.25$ and 0.5 for $\mu = \mu_1$.

Additional information can be obtained on the surface cleanness by measuring the secondary-emission coefficient γ_i. The values of $\varkappa$ obtained with Xe^+ and polycrystalline materials enable one to use (2) to determine γ_i for other gases. The values of $\varkappa$ for pure polycrystalline materials agree satisfactorily with the values of $\varkappa$ recommended in [17]. To supplement the data of [4] we measured the work function for the solder side of the solar batteries $\varkappa = 4.12$ eV (Xe^+) and $\varkappa = 4.33$ eV (Xe^+) for tin. The recommended value of the work function in [17] for Sn is $\varkappa = 4.38$ eV. In the measurements, the probe characteristics were recorded beginning at about —250 V, which produced outgassing by ion bombardment.

Figure 2a gives values of γ_i found from (2) on bombarding polycrystalline Mo, Ta, and Pt with ions of helium, neon, nitrogen, argon, and krypton with energies of about 100 eV. Points 1 for polycrystalline Mo are our results, 2 represents the data of [18], 3 the values of γ_i measured in [7, 19], and 4 the results of [20]. For polycrystalline Ta (broken line) and Pt, the points 1 and 3 are from our measurements, while points 2 and 4 are the data of [7, 19]. Figure 2b illustrates the dependence of γ_i on $(h_i - 2\varkappa)$. The filled points are the data of [21], while points 1-15 are our results. We obtained the following values for polycrystalline silicon: $\gamma_i^{He^+} \approx 0.144$, $\gamma_i^{Ne^+} \approx 0.082$, $\gamma_i^{Ar^+} \approx 0.051$, and $\gamma_i^{N_2^+} \approx 0.037$. The values found for $\gamma_i^{N_2^+}$ agree with the result $\gamma_i^{N_2^+} \approx 0.1$ for metals and $\gamma_i^{N_2^+} \approx 0.03$ for semiconductors given in [1]. The measurements on γ_i together with data from other sources indicate that the surface state of these targets were satisfactory. This confirms that ion bombardment is effective in cleaning.

Figure 3 illustrates the effect of particle speed on the energy accommodation coefficient for normal incidence on Mo. For the Xe^+—Mo ($\mu = 1.37$) system, curve 1 gives results for $\alpha_i^{Xe^+}$ on polycrystalline Mo without allowance for the sputtering, while curve 2 does the same with allowance for sputtering [22]; the points on curve 3 are the values of α_i measured on Mo (100) with a single crystal [23]; the points on curve 4 are results on $\alpha_i^{Xe^+}$—Mo (100) from [24]; curve 5 gives calculated values of $\alpha_i^{Xe^+}$ for Mo (100) from [23]; and curve 6 gives measurements of $\alpha_i^{Xe^+}$ on polycrystalline molybdenum on our measurements. For the system Kr^+—Mo ($\mu = 0.875$) the points on curve 1 are measurements on α_i on polycrystalline Mo [22]; curve 2 gives values of $\alpha_i^{Kr^+}$ measured on an Mo (100) single crystal in [24]; curve 3 gives our data recorded with polycrystalline Mo; curve 4 gives calculated values of $\alpha_i^{Kr^+}$ on Mo (100) from [23]; and points 5 are calculations on α in simulating the collision of particles with a three-dimensional crystal of linked atoms [25]. For Ar^+ on Mo ($\mu = 0.417$), curve 1 gives measurements on α_i for polycrystalline Mo from [22], while the points on curve 2 are our data; curves 3-5 represent measurements on $\alpha_i^{Ar^+}$ for the (111), (100), and (110) faces of an Mo single crystal in [24]; and curves 6 and 7 give calculations on α for gas atoms interacting with a solid represented as a linear harmonic oscillator (curve 6) or a semiinfinite lattice of elastically linked atoms as performed from formulas (1.25) and (2.6) of [26]. Points 8 are calculated values of α^{Ar} for a solid represented as a planar square lattice [27], while points 9 are the data of [25]. For N_2^+ on Mo ($\mu = 0.292$), curve 1 shows our data, while points 2 are the calculated values of α^{N_2} on Mo represented as a planar square lattice [27], points 3 are the calculated data of [25], and curves 4 and 5 represent calculations from formulas (1.25) and (2.6) of [26], correspondingly. For the system Ne^+—Mo ($\mu = 0.208$), curve 1 represents our data, while points 2 represent the calculated values of [27], points 3 represent the data of [25], and curves 4 and 5 are by calculation from the formulas of [26].

In the calculations on α_i from (1.25) and (2.6) of [26], the characteristic temperature of Mo was taken as $\Theta_d = 380°K$ [28]. The error from using the other limiting value $\Theta_d = 450°K$ [29] in calculating α_i does not exceed about 5%.

To determine α_i for various particle energies, particularly for $W_i \ll (e|V^A| + \chi)$, we also used (1) and (2) of [4].

Figure 3 indicates that α_i tends to a limit as the ion speed increases. The trends in $\alpha_i = \alpha_i(u_\infty)$ for polycrystalline and single-crystal targets are similar, and in the range $u_\infty \approx 7$-15 km/sec they agree with numerical estimates [25-27, 30] for various models. The values of α_i measured for polycrystalline and single-crystal targets are fairly similar. This similarity in the α_i for Mo evidently indicates that the ratio of the atomic masses has the main effect in this velocity range, and the influence of this factor is probably responsible for the increase in α_i with the mass of the bombarding ion.

Figure 4 shows the effects of atomic mass on α_i for polycrystalline technical material at $u_\infty \approx 8.2$ km/sec and $\theta = 0$.

This effect is also evident for polycrystalline materials of atomic mass from 27 to 207 bombarded by Xe^+ (point 1), Kr^+ (point 2), Ar^+ (point 3), N_2^+ (point 4), Ne^+ (point 5), and He^+ (point 6) for $u_\infty \approx 10$ km/sec and $\theta = 0$, as shown in Fig. 5. The points 7 correspond to the calculated values of the energy-exchange coefficients when the gas atoms interact with a hard-sphere lattice [1], while points 8 characterize the energy transfer from the gas atoms to a soft-sphere lattice [1], points 9 being from calculations on the energy exchange for particles colliding with an ideal crystal [31], points 10 being calculations on

α for scattering by a planar square lattice [27], and points 11 being data from simulation of the interaction of gas atoms with a three-dimensional crystal composed of linked atoms [25]. The broken line indicates calculations on α for atomic particles interacting with a solid represented by a linear harmonic oscillator and a semiinfinite lattice of elastically coupled atoms [26, 32].

Figure 6 illustrates the variation in $\alpha_{Mo}^{N_2^+}$ (μ = 0.292) on inclined incidence: Points 1 are our data, while curve 2 is for scattering of gas atoms at a hard-sphere lattice with allowance for the contribution from second collisions [1], points 3 represent the change in the energy-exchange coefficient for atoms colliding with a soft-sphere lattice [1], points 4 represent $\alpha_i(\theta)$ for simple reflection by a hard-sphere lattice [1], curve 5 represents calculations on the accommodation coefficient when particles collide with a planar square lattice [27], curve 6 is the numerical data of [33] for μ = 0.3, and the broken line shows $\alpha_i/\alpha_0 \simeq \cos\theta$ [2]. The experimental data agree best with the approximation $\alpha_i = \alpha_0 \cos\theta$. A possible reason for the discrepancy between the experimental and theoretical values for $\alpha_i(\theta)$ on inclined incidence is the difference in state between the surfaces of atomically smooth ideal crystals for which the numerical estimates were made and the real polycrystalline targets used in the experiments, particularly differences in roughness. Evidence for this comes from estimates on the effects of roughness on $\alpha_i(\theta)$ [34]. Curves 5 and 7 of Fig. 6 illustrate the tendency for $\alpha_i = \alpha_i(\theta)$ to vary as the roughness increases for μ = 0.3 and $u_\infty \simeq$ 10 km/sec.

Figure 7a shows the effects of particle velocity on $\alpha_i(\theta)$ for μ = 0.417 for comparison, Fig. 7a shows also the calculated values of $\alpha_i(\theta)$ for $u_\infty \simeq$ 10 km/sec. Curve 1 gives our measurements on $\alpha_i^{Ar^+}$ for u_∞ = 10 km/sec with polycrystalline Mo, while the points on curve 2 are the calculated values of [30], and curve 3 characterizes the scattering of gas atoms by a soft-sphere lattice [1], curve 4 indicates the contribution from second collisions for a hard-sphere lattice [1], and curve 5 gives calculations on α for gas atoms interacting with a planar square lattice [27]. The broken line shows $\alpha_i/\alpha_0 = \cos\theta$ [2]. For $\mu \simeq 0.3$ there is a discrepancy between the experimental and theoretical values for $\alpha_i(\theta)$ at $u_\infty \simeq$ 10 km/sec, which persists here. Points 6 and 7 represent measurements of α_i for single-crystal Mo (110) at $u_\infty \simeq$ 19.8 and 22.2 km/sec. Curves 8, 9, and 10 give values of $\alpha_i^{Ar^+}$ measured on polycrystalline Mo for $u_\infty \simeq$ 22.2, 38.2, and 49.2 km/sec [23]. Figure 7b shows results for polycrystalline Mo exposed to He^+ (our measurements). Curve 1 gives measurements of $\alpha_i^{He^+}/\alpha_0$ for $u_\infty \simeq$ 10 km/sec, while the points on curve 2 represent measurements at $u_\infty \simeq$ 22 km/sec, and curve 3 represents α_i/α_0 measured at $u_\infty \simeq$ 31 km/sec. The points on curves 4-6 were determined at $u_\infty \simeq$ 39, 53, and 62 km/sec, correspondingly. The broken line as before corresponds to $\alpha_i/\alpha_0 = \cos\theta$. The tendency for $\alpha_i(\theta)$ to vary as the ion speed increases is similar to that found in [35] for polycrystalline Ag, Pt, and Au bombarded by atoms from a neutralized Ar beam with velocities in the range ~50-120 km/sec. It has also been pointed out [30] that $\alpha_i(\theta)$ may vary with the particle speed (Fig. 5).

The results on $\alpha_i(\theta)$ indicate that the following approximation applies for ions with various masses at $u_\infty \simeq$ 10 km/sec:

$$\alpha_i/\alpha_0 \simeq \cos\theta + 0.333(1 + 1/\alpha_0)^{-2}\sin^2\theta(1 - \cos\theta)|\sin\theta - \cos\theta|,$$

where α_0 corresponds to normal incidence. This relationship is characteristic of all the gas-polycrystalline material systems examined. The values of α_0 are given in Figs. 4 and 5. The target temperature in the measurements of α_i was $T_w \simeq$ 310-320°K.

LITERATURE CITED

1. R. G. Barantsev, The Interaction of a Low-Density Flowing Gas with a Surface [in Russian], Nauka, Moscow (1975).
2. F. Goodman and H. Wachman, Dynamics of Gas Scattering by Surfaces [Russian translation], Mir, Moscow (1980).
3. M. Roberts and C. Mackie, Chemistry of Metal–Gas Interfaces [Russian translation], Mir, Moscow (1981).
4. V. A. Shuvalov, N. P. Reznichenko, and A. V. Gavrilov, "A study of the interaction parameters for a flow of low-density plasma and an electrically conducting surface by the use of thermoanemometer probes," Teplofiz. Vys. Temp., 19, No. 3 (1981).
5. B. V. Filippov, "The interaction of gas ions with the surface of a metal," in: Low-Density Gas Aerodynamics [in Russian], No. 3, Leningrad State Univ. (1967).

6. M. Kaminskii, Atomic and Ionic Collisions at the Surfaces of Metals [Russian translation], Mir, Moscow (1967).
7. U. A. Arifov, Interactions of Atomic Particles with the Surfaces of Solids [in Russian], Nauka, Moscow (1968).
8. V. M. Kovtunenko, V. F. Kameko, and É. P. Yaskevich, Aerodynamics of Orbital Space Vehicles [in Russian], Naukova Dumka, Kiev (1977).
9. V. L. Granovskii, Electric Current in Gases [in Russian], Gostekhizdat, Moscow (1952).
10. W. J. Weber, R. J. Armstrong, and J. Trulsen, "Ion-beam diagnostics by means of an electron-saturated plane Langmuir probe," J. Appl. Phys., 50, No. 7 (1979).
11. J. R. Sanmartin, "End effect in Langmuir probe response under ionospheric satellite conditions," Phys. Fluids, 15, No. 6 (1972).
12. A. V. Kolosov and S. G. Mironov, "Scattering of argon atoms of energy 0.15-1.8 eV by germanium," Zh. Prikl. Mekh. Tekh. Fiz., No. 4 (1976).
13. S. Morrison, Chemical Physics of Solid Surfaces [Russian translation], Mir, Moscow (1981).
14. A. R. Shul'man and S. A. Fridrikhov, Secondary-Emission Methods of Examining Solids [in Russian], Nauka, Moscow (1977).
15. G. I. Zakhar'in and G. V. Spivak, "Energy exchange between atoms of helium, neon, and argon with the surface of tungsten," Zh. Eksp. Teor. Fiz., 6, No. 10 (1936).
16. R. G. Barantsev and N. M. Moskaleva, "Scattering at an adsorbed layer," Vestn. Leningr. Gos. Univ., Ser. Mat., Mekh., Astron., No. 13, Issue 3 (1980).
17. V. S. Fomenko and I. A. Podchernyaeva, Emission and Adsorption Properties of Materials [in Russian], Atomizdat, Moscow (1975).
18. H. D. Hagstrum, "Auger ejection of electrons from molybdenum by noble gas ions," Phys. Rev., 104, No. 4 (1956).
19. U. A. Arifov and R. R. Rakhimov, "A study of the dependence of ion-electron emission on certain parameters of the target and bombarding ions," Izv. Akad. Nauk SSSR, Ser. Fiz., No. 6 (1960).
20. P. Mahadevan, J. K. Layton, and D. B. Medved, "Secondary electron emissions for clean surface of molybdenum due to low-energy noble gas ions," Phys. Rev., 129, No. 1 (1963).
21. A. I. Dobretsov and M. V. Gomoyunova, Emission Electronics [in Russian], Nauka, Moscow (1966).
22. K. I. Gusev, Yu. A. Ryzhov, and I. I. Shkarban, "Measurement of energy-accommodation coefficient in the bombardment of metals by inert-gas positive ions," in: Low-Density Gas Aerodynamics [in Russian], No. 7, Leningrad State Univ. (1974).
23. K. I. Gusev, D. S. Strizhenov, and I. I. Shkarban, "Energy exchange between a low-density flow with an energy of 80-500 eV and a surface," Trudy MAI, Issue 334 (1975).
24. K. I. Gusev, Yu. A. Ryzhov, et al., "The energy accommodation coefficient for particles incident on a solid at E_0 = 100-500 eV," Trudy MAI, Issue 351 (1976).
25. A. A. Pyarnpuu, "Calculation of the interaction between a monoenergetic beam of gas atoms and a three-dimensional crystal," Zh. Prikl. Mekh. Tekh. Fiz., No. 2 (1970).
26. A. I. Erofeev, "The interaction of fast particles with a solid," Uch. Zap. TsAGI, 1, No. 4 (1970).
27. A. I. Erofeev, "Exchange of energy and momentum between atoms and molecules in a gas and the surface of a solid," Zh. Prikl. Mekh. Tekh. Fiz., No. 2 (1967).
28. L. Zhirifal'ko, Statistical Solid-State Physics [Russian translation], Mir, Moscow (1975).
29. C. Kittel, Introduction to Solid State Physics, Wiley (1976).
30. Yu. A. Ryzhov and D. S. Strizhenov, "The interaction of atoms with a solid," Zh. Prikl. Mekh. Tekh. Fiz., No. 4 (1967).
31. Yu. A. Ryzhov and D. S. Strizhenov, "Energy exchange on interaction of atoms with an ideal crystal," Dokl. Akad. Nauk SSSR, 192, No. 6 (1967).
32. A. I. Erofeev and A. V. Zhbakova, "Calculation of collisions between gas atoms and surfaces for various solid-state models," Uch. Zap. TsAGI, 3, No. 5 (1972).
33. A. A. Pyarnpuu, "Models for the interaction of a low-density gas with a surface," in: Numerical Methods in the Theory of Low-Density Gases [in Russian], VTs Akad. Nauk SSSR, Moscow (1969).
34. A. I. Erofeev, "The effects of roughness on the interaction of a gas flow with a solid," Izv. Akad. Nauk SSSR, Mekh. Zhidk. Gaza, No. 6 (1967).
35. F. M. Devienne, "Variation of the accommodation coefficient of high-energy molecules on metal in terms of different parameters," in: Rarefied Gas Dynamics, Vol. 2, Academic Press, New York–London (1966).